HHS Public Access

Author manuscript

Cell. Author manuscript; available in PMC 2016 September 10.

Published in final edited form as:

Cell. 2015 September 10; 162(6): 1391–1403. doi:10.1016/j.cell.2015.08.024.

Ankyrin Repeats Convey Force to Gate the NOMPC Mechanotransduction Channel

Wei Zhang[1,3], **Li E. Cheng**[1,3], **Maike Kittelmann**[2,3,4], **Jiefu Li**[1], **Maja Petkovic**[1], **Tong Cheng**[1], **Peng Jin**[1], **Zhenhao Guo**[1], **Martin C. Göpfert**[2], **Lily Yeh Jan**[1], and **Yuh Nung Jan**[1,*]

[1]Howard Hughes Medical Institute, Departments of Physiology, Biochemistry and Biophysics, University of California, San Francisco, San Francisco, CA 94158, USA

[2]Department of Cellular Neurobiology, University of Göttingen, 37077 Göttingen, Germany

Summary

How metazoan mechanotransduction channels sense mechanical stimuli is not well understood. NOMPC channel in the transient receptor potential (TRP) family, a mechanotransduction channel for *Drosophila* touch sensation and hearing, contains 29 Ankyrin repeats (ARs) that associate with microtubules. These ARs have been postulated to act as a tether that conveys force to the channel. Here, we report that these N-terminal ARs form a cytoplasmic domain essential for NOMPC mechanogating *in vitro*, mechanosensitivity of touch receptor neurons *in vivo*, and touch-induced behaviors of *Drosophila* larvae. Duplicating the ARs elongates the filaments that tether NOMPC to microtubules in mechanosensory neurons. Moreover, microtubule association is required for NOMPC mechanogating. Importantly, transferring the NOMPC ARs to mechano-insensitive voltage-gated potassium channels confers mechanosensitivity to the chimeric channels. These experiments strongly support a tether mechanism of mechanogating for the NOMPC channel, providing insights regarding the basis of mechanosensitivity of mechanotransduction channels.

Graphical Abstract

[*]Correspondence to: yuhnung.jan@ucsf.edu.

[3]Co-first authors

[4]Present address: Oxford Brookes University, Plant Cell Biology, Gipsy lane, Oxford, OX3 0BP, UK.

Author Contributions

W. Z., L. E. C. and M. K. conducted most experiments. J. L. and T. C. made the chimeric constructs. M. P., P. J. and Z. G. helped on protein purification and biochemical assay. W. Z., M. K., M. C. G., L. Y. J. and Y. N. J. wrote the manuscript. All authors discussed the results and commented on the manuscript.

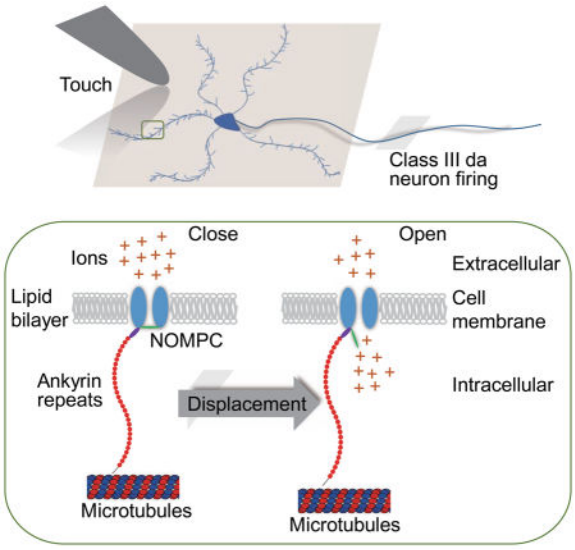

Introduction

Mechanotransduction channels convert mechanical stimuli into neuronal signals (Arnadottir and Chalfie, 2010; Coste et al., 2012; Vollrath et al., 2007). Several models have been proposed regarding how the mechanical force triggers channel opening (Kung, 2005; Lumpkin and Caterina, 2007; Orr et al., 2006). In the membrane force model, the force exerted via lipids in the membrane gates the channel. Alternatively, the tether model posits that the channel is tethered to intra- and/or extracellular structures and the force that is exerted by these molecular tethers gates the channel (Gillespie and Walker, 2001; Orr et al., 2006). Those models are not mutually exclusive as the cell membrane and tethers may act in concert in transmitting forces to the channel gate. While there is considerable evidence supporting the membrane force model for the bacterial MscL channel (Anishkin and Kung, 2013) and eukaryotic potassium channels (Brohawn et al., 2014a; Brohawn et al., 2012; Brohawn et al., 2014b; Lolicato et al., 2014), direct molecular evidence for the tether model has been lacking.

In the tether model, both rigid and elastic cellular components are required to couple stimulus-induced displacements to the membrane-bound channel (Lumpkin and Caterina, 2007). The rigid structures are thought to be composed of intracellular cytoskeletal elements and/or extracellular matrix components (Anishkin and Kung, 2013; Kung, 2005), and microtubules have been found to be essential for the mechanogating of TRPV1 channels on cells undergoing hypertonicity-induced shrinking (Prager-Khoutorsky et al., 2014). The molecular identities of the elastic components that transduce mechanical force to the channels and promote channel gating, however, remain unknown. Protein motifs that exhibit a certain level of elasticity have been suggested to function as gating springs that pulls open the channels during mechanotransduction. The stomatin-related protein Mec-2 in the MEC channel complex of *C. elegans* touch receptors (Goodman et al., 2002; Hu et al., 2010), tip link proteins in vertebrate hair cells (Grillet et al., 2009; Morgan and Barr-Gillespie, 2013; Phillips et al., 2008) and Ankyrin repeats (ARs) domain of some TRP channels (Gaudet,

2008; Howard and Bechstedt, 2004; Jin et al., 2006; Sotomayor et al., 2005b) are all candidates for such elastic tethers. The Ankyrin domain of 33 residues is a structural motif implicated in protein-protein interactions (Gaudet, 2008; Jin et al., 2006; Lee et al., 2006; Yang et al., 1998). Domains with a large tandem array of ARs resemble a coil with elasticity (Gaudet, 2008), making them intriguing candidates.

Among all known TRP channels, the NOMPC channel has the largest number of ARs (Montell, 2004, 2005), which are important for NOMPC functions in larval locomotion (Cheng et al., 2010). NOMPC fulfills essentially all the criteria for a *bona fide* mechanotransduction channel and mediates touch sensation in *Drosophila* larvae (Arnadottir and Chalfie, 2010; Yan et al., 2013). NOMPC is also involved in hearing of *Drosophila* larvae and adults (Bechstedt and Howard, 2008; Effertz et al., 2011; Kamikouchi et al., 2009; Lehnert et al., 2013; Liang et al., 2011; Zhang et al., 2013), collective behavior of adult flies (Ramdya et al., 2015), proprioception at adult leg joints (Chadha et al., 2015), as well as tension sensing in the hindgut of larvae (Zhang et al., 2014). NOMPC forms functional mechanotransduction channels in heterologous expression systems (Gong et al., 2013; Yan et al., 2013), thus facilitating structure-function studies of its mechanosensitivity (Zanini and Göpfert, 2013). These favorable features of NOMPC provide an opportunity to test the involvement of ARs, possibly functioning as a tether, in mechanotransduction.

In this study, we tested NOMPC mutants with various deletion or duplication of ARs and found that the integrity of 29 ARs is important for mechanogating of NOMPC in expression systems *in vitro* and in touch receptor neurons *in vivo*, since only NOMPC constructs with one or two complete sets of 29 ARs are mechanosensitive and effective in mediating touch-induced larval behavior. Having found that ARs associate with microtubules and doubling the ARs of NOMPC in mechanosensory campaniform sensilla results in lengthening of the membrane-microtubule connectors, we further showed that microtubule association is essential for NOMPC mechanosensitivity. To test whether ARs could confer mechanosensitivity, we transferred ARs from NOMPC to the voltage-gated potassium channel Kv1.2 and Kv2.1 that normally show little or no mechanosensitivity, and found that the chimeric channels respond to mechanical force with dose-dependent activation beyond the level achievable with depolarization. These findings provide strong evidence for the ability of ARs to mediate mechanosensitivity by functioning as a tether linking the channel and the microtubules and thus provide a precedent of the tether mechanism of mechanogating.

Results

The Ankyrin repeats are a cytoplasmic domain of NOMPC

To investigate the function of ARs in the N-terminus of NOMPC, we first assessed its localization relative to the cell membrane. Topological modeling indicated that NOMPC bears either 6 or 7 trans-membrane segments (Figure S1). To elucidate the topology of NOMPC, we employed antibodies recognizing different regions of NOMPC protein for immunostaining of cells in either permeabilized or non-permeabilized conditions. Surface expression of NOMPC in transfected S2 cells was confirmed with an antibody against an extracellular epitope in the putative pore region of NOMPC (αNOMPC-EC, Figure 1A),

which recognized NOMPC in the plasma membrane in the non-permeabilized condition (Figure 1B and Movie S1). We found that both the N-terminus and the C-terminus of NOMPC are on the cytoplasmic side of the membrane, since antibodies against the N-terminus of NOMPC (αNOMPC-N-ter, Figure 1A) (Liang et al., 2011) or the C-terminus of NOMPC (αNOMPC-C-ter, Figure 1A) (Cheng et al., 2010) immunostained permeabilized, but not non-permeabilized cells (Figures 1B and 1C). These results suggest a topology of NOMPC with 6 transmembrane helices and intracellular N- and C-termini (Figure 1A), which is typical of TRP channels (Venkatachalam and Montell, 2007).

ARs structure is essential for NOMPC surface expression

Immunostaining of NOMPC on the cell membrane with antibodies recognizing the extracellular domain of NOMPC (αNOMPC-EC) revealed that deleting all 29 ARs of NOMPC abolished surface expression (Figure 1E). To study the differential roles of ARs, we generated truncated NOMPC channels with different numbers of ARs. Δ1-12 ARs, which contains a total of 17 ARs, was constructed to resemble the cold-sensitive TRPA1 channels that contain 14-18 ARs in their N terminus (Julius, 2013; Paulsen et al., 2015). Through molecular dynamics simulations using crystallographic structures, Somomayor *et al.* showed that proteins containing 12 and 17 ARs could both respond to small forces by changing the curvature of ARs (Sotomayor et al., 2005; Sotomayor and Schulten, 2007). Δ13-29ARs (which contains the first 12 ARs) was constructed to test if there is a difference between these two blocks of ARs. NOMPC channel surface expression was abolished when the last 17 ARs (Δ13-29ARs-NOMPC) or the last 14 ARs (Δ16-29ARs-NOMPC) were deleted (Figures 1F and 1G). In contrast, deleting the first 12 ARs led to greater surface expression of NOMPC (Δ1-12ARs-NOMPC) and a higher open probability (Figures 1H, S2A and S2B), whereas swapping the first 12 ARs and the last 17 ARs of NOMPC abolished surface expression (Figure 1I). Duplicating the ARs in NOMPC (29+29ARs-NOMPC) was compatible with surface expression (Figure 1J), as was the addition of 17 ARs inserted near the first trans-membrane segment (TM1) of NOMPC (29+17ARs-NOMPC) (Figure 1K). It appears that most of the ARs, especially these preceding the trans-membrane segments, are required for NOMPC protein folding, assembly or membrane targeting. Furthermore, only those mutant and wild-type NOMPC proteins that displayed surface expression exhibited spontaneous channel activity (Figures 1D–1K).

Integrity of ARs is required for mechanotransduction by NOMPC channels

The ARs of NOMPC have been proposed to mediate the gating of mechanotransduction channels (Howard and Bechstedt, 2004; Sotomayor et al., 2005a). To test this possibility, we recorded from outside-out patches excised from transfected S2 cells and stimulated the membrane patches that were held at a specific voltage level with a brief negative pressure (50 mmHg) applied via a high speed pressure clamp.

Among those mutant NOMPC channels with membrane expression, only NOMPC with duplicated ARs (29+29ARs-NOMPC) exhibited mechanogating (Figures 2A and 2B). Whereas current amplitude normalized to patch membrane area as determined by membrane capacitance suggested the current mediated by wild-type NOMPC was larger than that mediated by NOMPC with duplicated ARs (Figure 2C, red bars), normalizing the

mechanosensitive current amplitude by the level of surface expression revealed that the mechanosensitive current response of NOMPC with duplicated ARs was comparable to that of wild-type NOMPC (Figure 2C, black bars). In contrast, deforming the membrane with the same pressure did not evoke responses of mutant Δ1-12ARs-NOMPC or 29+17ARs-NOMPC (Figures 2A–2C), even though both proteins exhibited surface expression and spontaneous channel activities. The spontaneous channel activities were likely from NOMPC channels, since they showed similar single channel conductance (Figure S2B) and could be blocked with the same channel blocker Gd^{3+} (Figure S2C).

Similar results were obtained when the S2 cells were stimulated with a piezo-actuator and the responses were recorded at the whole-cell configuration (Figure 2D). The amplitude of these mechanogated currents depended on the strength of mechanical stimulation (Figures 2E and 2F). Notably, the Δ1-12ARs-NOMPC exhibited a larger open probability than wild-type NOMPC in the absence of mechanical stimulation (Figures S2A and S2B). Thus, the integrity of the structure of 29 ARs from NOMPC is essential for mechanogating, possibly by forming a full turn of a helix for force transduction (Howard and Bechstedt, 2004). The requirement of all 29 ARs for NOMPC mechanogating might also explain why the number of ARs (29) is conserved across NOMPC homologues in fly, nematodes, zebrafish and frogs (Kang et al., 2010; Sidi et al., 2003).

ARs are required for NOMPC channel functions *in vivo*

Class III dendritic arborization (da) neurons in the *Drosophila* larval body wall rely on mechanotransduction by NOMPC to sense gentle touch (Yan et al., 2013). Null mutations of *nompC* abolish touch-evoked response of these neurons. To study the functional role of NOMPC ARs in these mechanosensory neurons, we tested whether NOMPC channels with different numbers of ARs driven by a class III da neurons specific Gal4 driver (19-12-Gal4) can functionally rescue touch-sensitivity in the *nompC* null mutant background. The GFP-tagged mutant NOMPC channels showed expression throughout the dendritic arborizations of the neurons, similar to that of wild-type NOMPC (Figure 3A). Non-permeabilized immunostaining of larval neurons revealed that both wild-type and 29+29ARs-NOMPC could be trafficked to the plasma membrane of dendrites. However, the expression level of 29+29ARs-NOMPC in class III da neurons was lower than that of wild-type NOMPC (Figures S3A and S3B), similar to what was observed in heterologous cells (Figures 1J). A single touch displacing the body wall by 20 μm triggered the firing of multiple action potentials of class III da neurons in wild-type but not *nompC* mutant larvae (Figures 3B and 3C). Expression in class III da neurons of wild-type NOMPC or NOMPC with duplicated ARs (29+29ARs) but not NOMPC with 29+17ARs, Δ1-29ARs or Δ1-12ARs rescued the mutant phenotype on touch-evoked response (Figures 3B and 3C). The partial rescue of NOMPC with 29+29ARs might be due to a lower expression level (Figures S3A and S3B). Together with our *in vitro* results shown in Figure 2, these findings illustrate that the integrity of the 29 ARs is essential for the mechanosensory function of NOMPC channels *in vivo* and the ability of class III da neurons to respond to gentle touch.

NOMPC mediated larval touch sensation requires ARs

Drosophila 3rd instar larvae show stereotyped behavioral responses to gentle touch that are mediated by the class III da neurons (Tsubouchi et al., 2012; Yan et al., 2013). Compared to the gentle touch response of wild-type controls, *nompC* null mutant larvae displayed a greatly reduced touch response (Figure 3D). Expressing wild type NOMPC, but not NOMPC channels with Δ1-29ARs, Δ1-12ARs or 29+17ARs, in the class III da neurons of *nompC* null mutants restored their touch sensitivity (Figure 3D). NOMPC channels with 29+29ARs could partially rescue touch sensation (Figure 3D), in accord with their lower capability of inducing mechanosensitive responses in S2 cells and class III da neurons (Figures 2E, 2F and 3C). Thus, in addition to being essential for NOMPC mechanogating and mechanically evoked neuronal response of sensory neurons, NOMPC ARs are required for behavioral responses to touch stimuli.

ARs are an essential component for membrane-microtubule connectors

Mechanosensory campaniform sensilla in the *Drosophila* haltere bear filamentous connections between the plasma membrane and the microtubule cytoskeleton, known as membrane-microtubule connectors (MMCs). These MMCs have been suggested to represent the ARs domain of NOMPC, tethering the channel to the microtubules (Liang et al., 2013). This raises the prospect that ARs might anchor to the microtubules and play a role in mechanical transduction (Zanini and Göpfert, 2013). Because of the favorable anatomy of campaniform sensilla in the *Drosophila* haltere whose dendritic tips are packed with NOMPC and whose MMCs are arranged in a regular array that can be discerned with EM (Figure 4A), we used these sensory organs to test whether the ARs of NOMPC might be visualized as a tether. Consistent with previous observations (Liang et al., 2013), we found that MMCs were indeed present in wild-type flies ('$NOMPC^{+}$') but virtually lost in $nompC^{1}$ null mutants ('$NOMPC^{-}$') (Figures 4A–4C and S4). In $nompC^{1}$ mutants, the MMCs were restored by expressing 29+29ARs-NOMPC in the receptors via nompC-GAL4, indicating that 29+29ARs-NOMPC integrates properly with its duplicated ARs domain binding microtubules (Figures 4A–4C and S4). Replacing wild-type NOMPC with 29+29ARs-NOMPC yielded significantly longer MMCs (mean MMC length ± S.D.: 18 ± 5 nm ($NOMPC^{29+29ARs}$) vs. 15 ± 5 nm ($NOMPC^{+}$)) (Figures 4D and S4) and a larger spacing between the membrane and the microtubule (mean distance ± S.D.: 15 ± 4 nm ($NOMPC^{29+29ARs}$) vs. 12 ± 4 nm ($NOMPC^{+}$)) (Figure 4D).

A priori, we had not expected that replacing wild-type NOMPC with 29+29ARs-NOMPC would cause such ultra-structural effects; loss of NOMPC protein reportedly leaves the microtubule-membrane distance largely unaffected (Liang et al., 2013), suggesting that the MMCs adjust their tension to fit into this pre-set distance (Zanini and Göpfert, 2013). However, when we systematically analyzed the membrane-microtubule distance in $NOMPC^{+}$ and $NOMPC^{-}$ flies, we found that this distance was slightly, yet significantly larger in *nompC* null mutants (mean distance ± S.D.: 17 ± 5 nm ($NOMPC^{-}$) vs. 12 ± 4 nm ($NOMPC^{+}$)) (Figure 4D). It thus appears that the MMCs pull together the membrane and the microtubules, explaining why changes in their spacing and in the MMC length can be discerned when NOMPC is replaced with 29+29ARs-NOMPC. In flies expressing 29+29ARs-NOMPC, the distribution of microtubule-membrane distances were significantly

different from those observed in NOMPC^{+} and NOMPC^{-} flies (Figure 4D), assuming intermediate values.

Microtubule is required for mechanogating of NOMPC channels

Heterologously expressed NOMPC proteins reportedly also associate with microtubules in cultured cells (Cheng et al., 2010). Double immune-labeling of NOMPC and microtubules revealed co-localization of NOMPC and microtubules in transfected S2 cells, especially in areas near the cell surface (Figure 5A). Staining of non-permeabilized cells with NOMPC antibody (αNOMPC-EC) further revealed that NOMPC channels on the plasma membrane co-localized with microtubules (Figure 5B). Furthermore, TIRF (Total Internal Reflection Fluorescence) microscopy imaging of the non-permeabilized staining is consistent with the notion that surface NOMPC channels interact with cortical microtubules in the vicinity of the membrane (Figures 5C and S5A). NOMPC expression in S2 cells did not alter the microtubule distribution (Figure S5B). To test whether NOMPC proteins bind to microtubules, we carried out the co-sedimentation assay. We found that wild-type NOMPC proteins from lysate of cells transfected with NOMPC associate with microtubules (Figure 5D). Furthermore, affinity purified NOMPC proteins (Figure S5C) also interacted strongly with microtubules (Figure 5D), indicating that NOMPC channels may bind to microtubules in cells.

In light of a recent report implicating interactions between TRPV1 channels and microtubules in osmotically induced cell shrinkage (Prager-Khoutorsky et al., 2014), we tested whether microtubules are required for mechanogating of NOMPC. Applying 100 nM of the microtubule depolymerizing drug nocodazole (Vasquez et al., 1997) to the cytoplasmic side of the S2 cell membrane in inside-out patches drastically reduced the NOMPC current response to mechanical stimuli, shortly after the onset of nocodazole infusion (Figure 5E). Nocodazole also had a similar effect when tested in the cell-attached mode (Figures 5F and 5G). Nocodazole treatment had no effect on NOMPC expression levels in the plasma membrane as revealed by NOMPC surface staining (Figures S5D and S5E). Nocodazole specifically reduced the NOMPC mechanogated current without affecting voltage-gating of Kv1.2 and Kv2.1 channels (Figures S5F–S5I). A chemically-unrelated microtubule depolymerizing drug colcemid had a similar effect on NOMPC channel gating, whereas enhancing microtubule polymerization with paclitaxel did not interfere with NOMPC activity (Figure 5H), further indicating that microtubules are essential for NOMPC mechanogating. In contrast, either stabilizing or disrupting the actin cytoskeleton had no effect on NOMPC mechanogating (Figure 5I). These findings indicate that NOMPC mechanosensitivity critically depends on the integrity of microtubules.

ARs transferred from NOMPC to Kv channels confer mechanosensitivity

Lastly, we tested if transferring the ARs from NOMPC to other ion channels could confer mechanosensitivity. We first chose as a recipient the mouse Kv1.2 voltage-gated potassium channel with a structure (Long et al., 2005) bearing architectural similarity with that of TRP channels (Kalia and Swartz, 2013). We constructed a chimeric protein by fusing the NOMPC N-terminal cytosolic domain including the 29 ARs (M1-S1268 from NOMPC) with the Kv1.2 transmembrane (TM) domain and C-terminus (G160-V499 from Kv1.2)

(S1268-G160-Kv1.2 chimera) (Figure 6A). To test if mechanical stimuli gate this chimeric channel, we applied 50 mmHg pressure to outside-out patches obtained from transfected S2 cells. Mechanically evoked currents were detected in K^+ but not Cs^+ containing intracellular solutions, when the membrane potential was held at +60 mV (Figures 6B and 6C). By contrast, no mechanosensitive current was detectable in patches with wild-type Kv1.2 or Kv1.2 without its N-terminal cytosolic domain (Kv1.2ΔNterminus) (Figures 6B and 6C). Our experiments further revealed that the pre-S1 linker of NOMPC is important for mechanotransduction since a chimeric channel containing the NOMPC ARs but not this linker (M1-M1120 from NOMPC) and the Kv1.2 TM domain and C-terminus (G160-V499 from Kv1.2) (M1120-G160-Kv1.2 chimera) was not mechanosensitive (Figures 6B and 6C). To corroborate that the mechanosensitive current indeed originated from the S1268-G160-Kv1.2 chimera, we tested the specific Kv1.2 channel blocker maurotoxin (MTX) (Kharrat et al., 1997), which blocked the mechanosensitive current of the chimeric channel (Figure 6D), while having no effect on NOMPC channel activity (Figures S6A and S6B).

Kv1.2 was reported to be slightly mechanosensitive when stimulated with a piezo actuator (Hao et al., 2013) even though it was not mechanosensitive in our assay system (Figures 6B and 6C). To further validate that ARs are capable of conferring mechanosensitivity, we constructed chimeric channels by transferring ARs from NOMPC to the trans-membrane domain and C-terminus of another voltage-gated K^+ channel Kv2.1 (Figure 6A), which was reported to show no mechanosensitivity (Hao et al., 2013). Again, the chimeric channel (S1268-V182-Kv2.1 chimera) exhibited mechanosensitivity similar to that of ARs-Kv1.2 chimeric channels whereas wild-type Kv2.1, Kv2.1 lacking the N-terminal cytosolic domain (Kv2.1ΔNterminus) and a chimeric channel containing the NOMPC ARs but not the linker and the Kv2.1 TM domain and C-terminus (M1120-G182-Kv2.1 chimera) were not mechanosensitive (Figures 6E and 6F).

Chimeric channels share similar gating mechanisms with NOMPC

Dose-dependent responses to mechanical stimuli and adaptation to prolonged mechanical stimulation are hallmarks of mechanosensitivity. Both chimeric channels showed dose-dependent responses when stimulated with different levels of pressure applied to the membrane, similar to that of NOMPC channels. The current amplitudes increased progressively with the pressure intensity (Figures 7A and S7A). The chimeric channels appeared to exhibit a lower current amplitude to pressure as compared to wild-type NOMPC (Figures 2E, 7B and S7B). Mechanosensitive currents from the S1268-G160-Kv1.2 chimera exhibited adaptation in response to maintained pressure stimulation (Figure 7C).

Next, we wanted to know whether the mechanosensitive currents of the chimeric channels depends on their interacting with microtubules. Similar to NOMPC channels, the chimeric channels exhibited microtubule interaction, which was more prominent than that of wild-type Kv channels (Figures 7E and S7C). The mechanogated current from ARs-Kv1.2 chimeric channels also depended on microtubule integrity, since disrupting microtubules with nocodazole largely abolished the mechanical response of the chimeric channels (Figure 7D), while leaving voltage-gating of wild-type Kv1.2 channels unaffected (Figures S5F and

S5G). These experiments provide further support that ARs are part of a tether that links the channels with microtubules.

Without the Kv1.2 or Kv2.1 N-terminus that includes the T1 tetramerization domain, the chimeric channels yielded smaller currents, and the voltage dependence of the normalized current (I/I_{max}) was shifted to the right for both Kv1.2 (Figures 7F–7H) and Kv2.1 (Figures 7I–7K). By applying a 50 mmHg pressure pulse to patches with ARs-Kv chimeric channels during each membrane depolarization step, we normalized the current at the plateau phase near the end of the depolarization as well as the current during the pressure pulse to the current induced by depolarization to +100 mV (I_{max}) (Figures 7H and 7K). This revealed a synergistic action of voltage gating and mechanogating. Mechanical stimulation shifted the I–V curve of ARs-Kv channels to the left while having no effect on wild-type Kv channels at any voltage tested, leaving the $V_{1/2}$ unchanged, which was 12.1 mV for Kv1.2 (Figure 7H) and 28 mV for Kv2.1 (Figure 7K). It thus appears that transferring the ARs of NOMPC confers mechanosensitivity to the chimeric channel containing the voltage sensor and the pore of Kv1.2 or Kv2.1, by allowing the chimeric channels to respond to mechanical force and activate to a greater extent than what could be achieved by depolarization.

Discussion

In this study, we have provided evidence that ARs are essential for NOMPC mechanogating. We further show that mechanogating of NOMPC requires the integrity of microtubules associated to the plasma membrane, providing a precedent for a tethered mechanism for mechanotransduction channel activation. That the ARs of NOMPC can render voltage-gated potassium channels mechanosensitive highlights their functional sufficiency for mechanogating for those normally mechano-insensitive channels.

The components of MMCs

Documenting that duplicating the NOMPC ARs elongates the MMCs, our analysis supports previous indications (Liang et al., 2013) that the ARs are the main components of the MMCs. Based on our analysis, duplicating the ARs elongates the MMCs by ca. 20%, but does not duplicate their length. Possibly, the length increase is underestimated when being assayed only in a two-dimensional plane, and adjacent Ankyrins might also have moved closer together, which cannot be resolved by electron-microscopy. Alternatively, it seems likely that the MMC length is constrained by the membrane-microtubule distance, and that the MMCs are fit into this pre-set distance by adjusting their tension rather than their length. Measured membrane-microtubule distances are larger for $NOMPC^{-}$ than for $NOMPC^{+}$ flies, suggesting that the membrane and the microtubules are pulled together by the MMCs. Upon duplication of the ARs, the membrane-microtubule distance assumes intermediate values in between those of $NOMPC^{-}$ and $NOMPC^{+}$ flies, pointing to a reduced pull by – and a reduced stiffness of – the MMCs.

Hence, although the membrane-microtubule distance remains largely unaltered when NOMPC is lost (Liang et al., 2013), the slight change that shows up when large numbers of sensilla are analyzed explains why we detected the MMC elongation that arises when NOMPC is replaced by 29+29ARs-NOMPC.

The regulation of NOMPC gating by other cellular components

Heterologous expression of NOMPC expression in S2 cells is sufficient to generate mechanosensitive channels. However, NOMPC channels and their homologs may serve multiple functions in different mechanosensors (Chadha et al., 2015; Effertz et al., 2011; Kang et al., 2010; Lehnert et al., 2013; Ramdya et al., 2015; Sidi et al., 2003; Yan et al., 2013; Zhang et al., 2013; Zhang et al., 2014), and their functions may be regulated differently in different cell types. It is conceivable that in different mechanosensors, NOMPC interacts with different sets of molecules that regulate channel opening *in vivo*, a possibility that warrants future investigation for better understanding of the mechanical gating machinery. Notably, Ankyrin domain is a motif for mediating protein-protein interactions in various biological processes, raising the possibility that other proteins bind to ARs to regulate NOMPC channel functions.

Our current findings support a tether model, in which NOMPC channels dock to intracellular cytoskeleton via their ARs that form the gating tethers. There are two different versions of the tether model: (1) an intracellular tether model and (2) a model involving both intracellular and extracellular tethers (Lumpkin and Caterina, 2007). In this study, we have provided strong evidence that ARs serve as an intracellular tether. It remains an open question whether there are any extracellular partners of NOMPC channels involved in their gating, either with direct or indirect interactions. NOMPA, a protein identified in the same genetic screen (Kernan et al., 1994) that also led to the discovery of NOMPC, is required for the normal development of chordotonal neurons in fly hearing organs (Boekhoff-Falk, 2005). Immunostaining of fly Johnston organs has shown that NOMPA localizes at the tip of chordotonal neurons and might play a role in docking the dendritic tips to their supporting cells (Chung et al., 2001). Further experiments would be needed to test whether NOMPC interacts with NOMPA or other proteins in the mechanosensory organs.

The transformation of mechanical forces to protein dynamics

Our finding that ARs from NOMPC can gate chimeric Kv channels with their N-termini replaced by these ARs, set the stage to create mechanotransduction channels/machineries by protein engineering. Compared to the chimeric channels, NOMPC is more susceptible to forces conveyed by ARs, raising the possibility that the trans-membrane domain of NOMPC is more amenable to mechanogating. We wish to emphasize that while our results strongly support the notion that ARs function as a tether for mechanogating of NOMPC, our results do not exclude the potential role of interactions between NOMPC protein and the membrane lipids nearby. Structural information of the NOMPC channel will be valuable for future investigation of force transmission and force-displacement conversion within a mechanotransduction channel protein as well as the potential roles of the lipid molecules in the membrane near NOMPC.

Experimental Procedures

Constructs of mutated NOMPC channels and mechanogated chimeric channels

To generate NOMPC Ankyrin repeats deletion or elongation constructs, a PCR based approach was used. The mutated NOMPC coding regions were cloned into pUAST vector

for cell transfection and transgenic fly injections. To generate the synthetic mechanogated potassium channels, fragments of NOMPC Ankyrin repeats and Kv1.2/Kv2.1 transmembrane domains were assembled into pAc5.1/V5-His A (Invitrogen) with C-terminus GFP by following the protocol of Gibson Assembly Kit (NEB). See Supplemental Experimental Procedures for construct sequences and primer information.

Immunostaining and microscopy

For non-permeabilized staining, the transfected cells were incubated with primary antibody before fixation. For permeabilized staining, cells were fixed and incubated with PBST for 10 min. The cells were then blocked and stained with primary and secondary antibodies. Larval body wall neuron staining was performed as reported previously (Grueber et al., 2002). See Supplemental Experimental Procedures for antibodies information and TIRF microscopy settings.

Biochemistry

Drosophila nompC gene was expressed in and purified from a baculovirus transduction-based system with HEK293S GnTi-cells. Cell lysate or purified protein of interest were added to the polymerized microtubules or resuspension buffer alone as negative control. The mix was incubated at room temperature for 20 min and spin 10 min. Supernatant and pellet resuspended in equal volume of the resuspension buffer were collected and analysed. See Supplemental Experimental Procedures for cell culture, protein purification and co-sedimentation details.

Immuno-electron microscopy

Halteres and attached fragments of the thorax were fixed and then dehydrated in an ethanol series including a block staining step. Infiltration was done for two days raising the Durcupan concentration from 30% to 90%. 70 nm ultrathin sections were cut and transferred onto copper mesh grids. Micrographs were taken with a JEOL electron microscope with a GatanOrius 1200A camera. See Supplemental Experimental Procedures for full TEM methods.

Electrophysiological recordings

Drosophila S2 cells were cultured in Schneider' *Drosophila* medium supplied with 5% FBS at 25 °C. Effectene Kit (Qiagen) was used to transfect cells according to the product protocol. Recordings were carried out 1–2 days after transfection. Drugs were dissolved in the bath solution to the final concentration right before experiments. The drug-containing solution was perfused to the recording chamber. Larval electrophysiological recordings were carried out as previously described (Yan et al., 2013). See Supplemental Experimental Procedures for sample preparation, recording solutions, drug concentrations and electrophysiological recording configurations.

Mechanical stimulation

A glass probe was driven by a piezo actuator to deliver mechanical stimulation. For larval body wall stimulation, the stimulation pipette was sealed and fire-polished to a diameter

around 20 μm. For cultured S2 cells, the pipette was sealed and polished by microforge to a diameter around 1 μm. Negative pressure was applied to the membrane patches via a High Speed Pressure Clamp (HSPC, ALA-scientific). See Supplemental Experimental Procedures for details on mechanical stimulation delivery.

Supplementary Material

Refer to Web version on PubMed Central for supplementary material.

Acknowledgments

We thank C. Zuker (Columbia University) for fly lines, J. Howard (Yale University) for a NOMPC antibody. We thank S. Q. Zhang and H. H. Yang for help on chimeric protein design, S. Yadav for assistance on antibody staining, D. Kamiyama and M. He for assistance on TIRF microscopy, J. Trimmer for Kv2.1 clones. S. Younger, S. Barbel, and M. Winkler for technical support, and members of the Jan and Göpfert labs for discussion. This work was supported by DFG grants (SPP 1608 GO 1092/2-1, GO 1092/1-2, and SFB 889 A1) to M.C.G., BRAINseed award to Y. N. J., A. P. and J. Y. W. and NIH grants (R37NS040929 and 5R01MH084234) to Y. N. J.. L. Y. J. and Y. N. J. are investigators of the Howard Hughes Medical Institute.

References

Anishkin A, Kung C. Stiffened lipid platforms at molecular force foci. Proc Natl Acad Sci U S A. 2013; 110:4886–4892. [PubMed: 23476066]

Arnadottir J, Chalfie M. Eukaryotic mechanosensitive channels. Annu Rev Biophys. 2010; 39:111–137. [PubMed: 20192782]

Bechstedt S, Howard J. Hearing mechanics: A fly in your ear. Curr Biol. 2008; 18:R869–R870. [PubMed: 18812084]

Boekhoff-Falk G. Hearing in *Drosophila*: development of Johnston's organ and emerging parallels to vertebrate ear development. Dev Dyn. 2005; 232:550–558. [PubMed: 15704117]

Brohawn SG, Campbell EB, MacKinnon R. Physical mechanism for gating and mechanosensitivity of the human TRAAK K+ channel. Nature. 2014a; 516:126–130. [PubMed: 25471887]

Brohawn SG, del Marmol J, MacKinnon R. Crystal structure of the human K2P TRAAK, a lipid- and mechano-sensitive K+ ion channel. Science. 2012; 335:436–441. [PubMed: 22282805]

Brohawn SG, Su Z, MacKinnon R. Mechanosensitivity is mediated directly by the lipid membrane in TRAAK and TREK1 K+ channels. Proc Natl Acad Sci U S A. 2014b; 111:3614–3619. [PubMed: 24550493]

Chadha A, Kaneko M, Cook B. NOMPC-dependent mechanotransduction shapes the dendrite of proprioceptive neurons. Neurosci Lett. 2015; 597:111–116. [PubMed: 25916878]

Cheng LE, Song W, Looger LL, Jan LY, Jan YN. The Role of the TRP Channel NompC in Drosophila Larval and Adult Locomotion. Neuron. 2010; 67:373–380. [PubMed: 20696376]

Chung YD, Zhu J, Han Y, Kernan MJ. nompA encodes a PNS-specific, ZP domain protein required to connect mechanosensory dendrites to sensory structures. Neuron. 2001; 29:415–428. [PubMed: 11239432]

Coste B, Xiao B, Santos JS, Syeda R, Grandl J, Spencer KS, Kim SE, Schmidt M, Mathur J, Dubin AE, et al. Piezo proteins are pore-forming subunits of mechanically activated channels. Nature. 2012; 483:176–181. [PubMed: 22343900]

Effertz T, Wiek R, Göpfert MC. NompC TRP channel is essential for Drosophila sound receptor function. Curr Biol. 2011; 21:592–597. [PubMed: 21458266]

Gaudet R. A primer on ankyrin repeat function in TRP channels and beyond. Mol Biosyst. 2008; 4:372–379. [PubMed: 18414734]

Gillespie PG, Walker RG. Molecular basis of mechanosensory transduction. Nature. 2001; 413:194–202. [PubMed: 11557988]

Gong JX, Wang QX, Wang ZR. NOMPC is likely a key component of Drosophila mechanotransduction channels. European Journal of Neuroscience. 2013; 38:2057–2064. [PubMed: 23590241]

Goodman MB, Ernstrom GG, Chelur DS, O'Hagan R, Yao CA, Chalfie M. MEC-2 regulates C. elegans DEG/ENaC channels needed for mechanosensation. Nature. 2002; 415:1039–1042. [PubMed: 11875573]

Grillet N, Kazmierczak P, Xiong W, Schwander M, Reynolds A, Sakaguchi H, Tokita J, Kachar B, Muller U. The mechanotransduction machinery of hair cells. Sci Signal. 2009; 2(pt5)

Grueber WB, Jan LY, Jan YN. Tiling of the Drosophila epidermis by multidendritic sensory neurons. Development. 2002; 129:2867–2878. [PubMed: 12050135]

Hao J, Padilla F, Dandonneau M, Lavebratt C, Lesage F, Noel J, Delmas P. Kv1.1 channels act as mechanical brake in the senses of touch and pain. Neuron. 2013; 77:899–914. [PubMed: 23473320]

Howard J, Bechstedt S. Hypothesis: a helix of ankyrin repeats of the NOMPC-TRP ion channel is the gating spring of mechanoreceptors. Curr Biol. 2004; 14:R224–226. [PubMed: 15043829]

Hu J, Chiang LY, Koch M, Lewin GR. Evidence for a protein tether involved in somatic touch. EMBO J. 2010; 29:855–867. [PubMed: 20075867]

Jin X, Touhey J, Gaudet R. Structure of the N-terminal ankyrin repeat domain of the TRPV2 ion channel. J Biol Chem. 2006; 281:25006–25010. [PubMed: 16809337]

Julius D. TRP channels and pain. Annu Rev Cell Dev Biol. 2013; 29:355–384. [PubMed: 24099085]

Kalia J, Swartz KJ. Exploring structure-function relationships between TRP and Kv channels. Sci Rep. 2013; 3:1523. [PubMed: 23519328]

Kamikouchi A, Inagaki HK, Effertz T, Hendrich O, Fiala A, Göpfert MC, Ito K. The neural basis of Drosophila gravity-sensing and hearing. Nature. 2009; 458:165–171. [PubMed: 19279630]

Kang L, Gao J, Schafer WR, Xie Z, Xu XZ. C. elegans TRP family protein TRP-4 is a pore-forming subunit of a native mechanotransduction channel. Neuron. 2010; 67:381–391. [PubMed: 20696377]

Kernan M, Cowan D, Zuker C. Genetic dissection of mechanosensory transduction: mechanoreception-defective mutations of Drosophila. Neuron. 1994; 12:1195–1206. [PubMed: 8011334]

Kharrat R, Mansuelle P, Sampieri F, Crest M, Oughideni R, Van Rietschoten J, Martin-Eauclaire MF, Rochat H, El Ayeb M. Maurotoxin, a four disulfide bridge toxin from Scorpio maurus venom: purification, structure and action on potassium channels. FEBS Lett. 1997; 406:284–290. [PubMed: 9136903]

Kung C. A possible unifying principle for mechanosensation. Nature. 2005; 436:647–654. [PubMed: 16079835]

Lee G, Abdi K, Jiang Y, Michaely P, Bennett V, Marszalek PE. Nanospring behaviour of ankyrin repeats. Nature. 2006; 440:246–249. [PubMed: 16415852]

Lehnert BP, Baker AE, Gaudry Q, Chiang AS, Wilson RI. Distinct roles of TRP channels in auditory transduction and amplification in Drosophila. Neuron. 2013; 77:115–128. [PubMed: 23312520]

Liang X, Madrid J, Gartner R, Verbavatz JM, Schiklenk C, Wilsch-Brauninger M, Bogdanova A, Stenger F, Voigt A, Howard J. A NOMPC-dependent membrane-microtubule connector is a candidate for the gating spring in fly mechanoreceptors. Curr Biol. 2013; 23:755–763. [PubMed: 23583554]

Liang X, Madrid J, Saleh HS, Howard J. NOMPC, a member of the TRP channel family, localizes to the tubular body and distal cilium of Drosophila campaniform and chordotonal receptor cells. Cytoskeleton (Hoboken). 2011; 68:1–7. [PubMed: 21069788]

Lolicato M, Riegelhaupt PM, Arrigoni C, Clark KA, Minor DL Jr. Transmembrane Helix Straightening and Buckling Underlies Activation of Mechanosensitive and Thermosensitive K2P Channels. Neuron. 2014; 84:1198–1212. [PubMed: 25500157]

Long SB, Campbell EB, Mackinnon R. Crystal structure of a mammalian voltage-dependent Shaker family K+ channel. Science. 2005; 309:897–903. [PubMed: 16002581]

Lumpkin EA, Caterina MJ. Mechanisms of sensory transduction in the skin. Nature. 2007; 445:858–865. [PubMed: 17314972]

Montell C. Molecular genetics of *Drosophila* TRP channels. Novartis Found Symp. 2004; 258:3–12. discussion 12–17, 98–102, 263-106. [PubMed: 15104173]

Montell C. *Drosophila* TRP channels. Pflugers Arch. 2005; 451:19–28. [PubMed: 15952038]

Morgan CP, Barr-Gillespie PG. Mechanotransduction: the elusive hair cell transduction channel revealed? Curr Biol. 2013; 23:R887–890. [PubMed: 24112987]

Orr AW, Helmke BP, Blackman BR, Schwartz MA. Mechanisms of mechanotransduction. Dev Cell. 2006; 10:11–20. [PubMed: 16399074]

Paulsen CE, Armache JP, Gao Y, Cheng Y, Julius D. Structure of the TRPA1 ion channel suggests regulatory mechanisms. Nature. 2015; 520:511–517. [PubMed: 25855297]

Phillips KR, Biswas A, Cyr JL. How hair cells hear: the molecular basis of hair-cell mechanotransduction. Curr Opin Otolaryngol Head Neck Surg. 2008; 16:445–451. [PubMed: 18797287]

Prager-Khoutorsky M, Khoutorsky A, Bourque CW. Unique Interweaved Microtubule Scaffold Mediates Osmosensory Transduction via Physical Interaction with TRPV1. Neuron. 2014; 83:866–878. [PubMed: 25123313]

Ramdya P, Lichocki P, Cruchet S, Frisch L, Tse W, Floreano D, Benton R. Mechanosensory interactions drive collective behaviour in Drosophila. Nature. 2015; 519:233–236. [PubMed: 25533959]

Sidi S, Friedrich RW, Nicolson T. NompC TRP channel required for vertebrate sensory hair cell mechanotransduction. Science. 2003; 301:96–99. [PubMed: 12805553]

Sotomayor M, Corey DP, Schulten K. In search of the hair-cell gating spring elastic properties of ankyrin and cadherin repeats. Structure. 2005a; 13:669–682. [PubMed: 15837205]

Sotomayor M, Corey DP, Schulten K. Molecular dynamics study of mechanosensation proteins ankyrin and cadherin. Biophysical Journal. 2005b; 88:288a–288a.

Tsubouchi A, Caldwell JC, Tracey WD. Dendritic filopodia, Ripped Pocket, NOMPC, and NMDARs contribute to the sense of touch in Drosophila larvae. Curr Biol. 2012; 22:2124–2134. [PubMed: 23103192]

Vasquez RJ, Howell B, Yvon AM, Wadsworth P, Cassimeris L. Nanomolar concentrations of nocodazole alter microtubule dynamic instability in vivo and in vitro. Mol Biol Cell. 1997; 8:973–985. [PubMed: 9201709]

Venkatachalam K, Montell C. TRP channels. Annu Rev Biochem. 2007; 76:387–417. [PubMed: 17579562]

Vollrath MA, Kwan KY, Corey DP. The micromachinery of mechanotransduction in hair cells. Annu Rev Neurosci. 2007; 30:339–365. [PubMed: 17428178]

Yan Z, Zhang W, He Y, Gorczyca D, Xiang Y, Cheng LE, Meltzer S, Jan LY, Jan YN. Drosophila NOMPC is a mechanotransduction channel subunit for gentle-touch sensation. Nature. 2013; 493:221–225. [PubMed: 23222543]

Yang Y, Nanduri S, Sen S, Qin J. The structural basis of ankyrin-like repeat function as revealed by the solution structure of myotrophin. Structure. 1998; 6:619–626. [PubMed: 9634699]

Zanini D, Göpfert MC. Mechanosensation: tethered ion channels. Curr Biol. 2013; 23:R349–351. [PubMed: 23660354]

Zhang W, Yan Z, Jan LY, Jan YN. Sound response mediated by the TRP channels NOMPC, NANCHUNG, and INACTIVE in chordotonal organs of Drosophila larvae. Proc Natl Acad Sci U S A. 2013; 110:13612–13617. [PubMed: 23898199]

Zhang W, Yan Z, Li B, Jan LY, Jan YN. Identification of motor neurons and a mechanosensitive sensory neuron in the defecation circuitry of larvae. Elife. 2014; 3:10. 7554/eLife.03293.

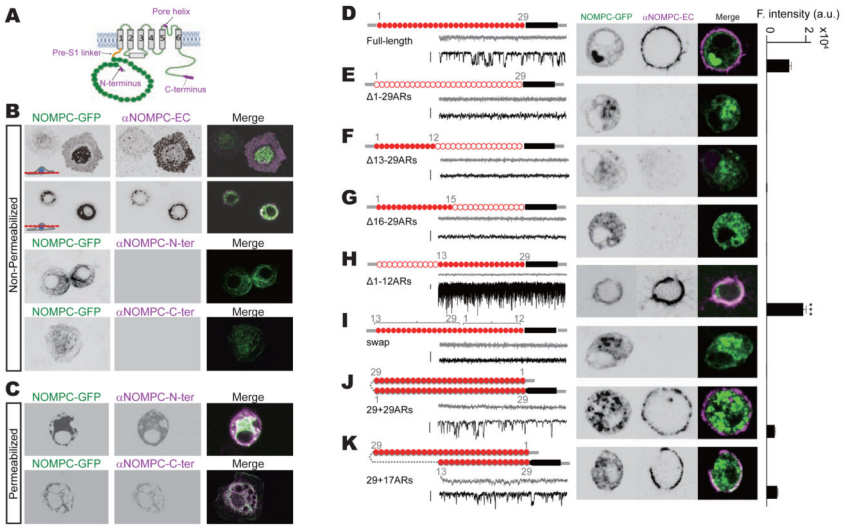

Figure 1. Ankyrin repeats are essential for NOMPC membrane expression

(A) A schematic topology of predicted architecture of a NOMPC channel subunit. Magenta tags indicate the epitopes recognized by antibodies used in this study. (B) Non-permeabilized staining of NOMPC protein with antibody against the pore helix (αNOMPC-EC), NOMPC N-terminus (αNOMPC-N-ter) and NOMPC C-terminus (αNOMPC-C-ter) (scale bar: 10 μm). (C) Permeabilized staining of NOMPC protein. (D to K) Schematic molecular architectures, surface staining (scale bar: 5 μm) and spontaneous channel activities (scale bar: 10 pA) of NOMPC channels with different number and arrangements of ARs. Filled red circles indicate an Ankyrin domain; empty red circles indicate a deleted Ankyrin domain; black bars indicate transmembrane segments; numbers (grey) indicate the original order of the Ankyrin domain. Current traces were obtained at holding potential of 0 mV (grey) and −60 mV (black) (scale bar: 10 pA). Bar plots on the right represent fluorescence intensity (F. intensity) of surface NOMPC staining (a.u.: arbitrary unit, n = 28, 10, 10, 11, 25, 12, 17 and 29. Paired *t*-test between time full-length and Δ1-12ARs-NOMPC, ***P3<30.001). (E to H) Different truncations of ARs produced channels with different extent of surface expression. (I) Swap of first 12 and last 17 ARs eliminated surface expression. (J and K) NOMPC with extra ARs have normal membrane targeting. All error bars denote ± s.e.m.. See also Figure S1 and Movie S1.

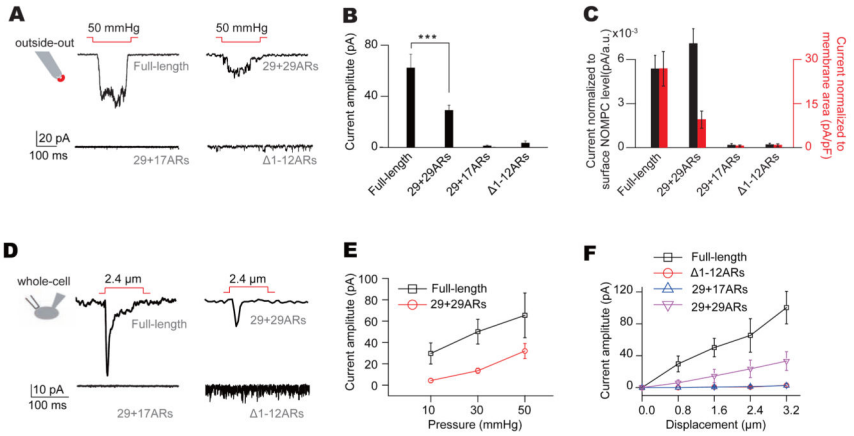

Figure 2. Integrity of Ankyrin repeats is required for NOMPC mechanogating

(A) Representative traces of mechanogated current from NOMPC channels with different number of ARs on an outside-out patch held at −60 mV. (B) Plots of mechanogated current amplitudes (absolute value) (n = 12, 11, 8 and 7. one-way analysis of variance followed by Tukey's comparison, ***P3<30.001). (C) Plots of mechanogated current amplitudes normalized to surface expression level (dark bars) and membrane capacitance (red bars) (n = 12, 11, 8 and 7. one-way analysis of variance followed by Tukey's comparison, ***P3<30.001). (D) Representative traces of mechanogated current triggered by piezo displacements from NOMPC channels with different number of ARs on a transfected cell held at −60 mV. (E and F) Dose-dependent curves of NOMPC mechanogated currents to pressure (E) (n = 10 and 7) and piezo displacements (F) (n = 10, 6, 8 and 7). All error bars denote ± s.e.m.. See also Figure S2.

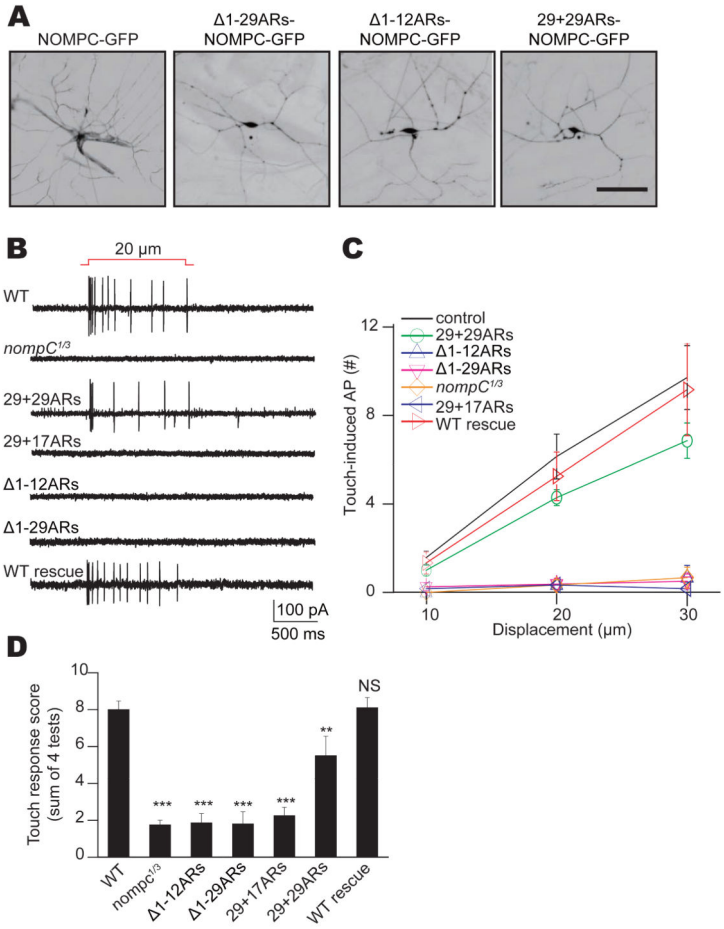

Figure 3. NOMPC channel functions *in vivo* require Ankyrin repeats

(A) Wild type and mutant NOMPC expression in class III da neurons of *nompC* null mutants (scale bar: 50 μm). (B) Class III da neurons' response to mechanical stimulation, revealing functional rescue of *nompC* null phenotype by full-length NOMPC and 29+29ARs-NOMPC, but not other mutated NOMPC channels. (C) Dose-dependent neuronal response to mechanical displacement of increasing distance on larval body wall. (D) Rescue of the deficient touch response of *nompC* null mutant larvae by expressing full-length NOMPC or 29+29ARs-NOMPC, but not other mutated NOMPC channels in their class III da neurons with a class III da neurons specific Gal4 driver (19-12-Gal4). We used unpaired *t*-test for comparison between two groups, and one-way analysis of variance followed by Tukey's comparison for analyses of three or four groups. N.S., not significant. **P3<30.01, ***P < 0.001. All error bars denote ± s.e.m.. Genotypes are as follows: control: w^{1118}. *nom: pC* $nompC^{1}/nompC^{3}$. WT rescue (full-length NOMPC): $nompC^{1}/nompC^{3}$; *19-12-Gal4*, *UAS-NOMPC-GFP*. Δ1-29ARs: $nompC^{1}/nompC^{3}$; *19-12-Gal4*/*UAS-Δ1-29ARs-NOMPC-GFP*. Δ1-12ARs: $nompC^{1}/nompC^{3}$; *19-12-Gal4*/*UAS-Δ1-12ARs-NOMPC-GFP*. 29+17ARs: $nompC^{1}/nompC^{3}$; *1 9-12-Gal4*, *UAS-29+17ARs-NOMPC-GFP*. 29+29ARS: $nompC^{1}/nompC^{3}$; *19- 12-Gal4*, *UAS-29+29ARs-NOMPC-GFP*. All flies are in *w* background. See also Figure S3.

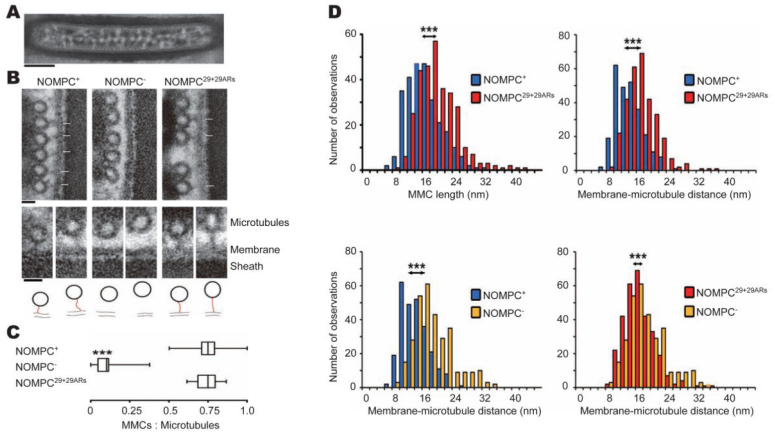

Figure 4. ARs are the essential component of membrane-microtubule connectors

(A) Overall structure the dendritic tip from haltere companionform sensillium (scale bar: 200 nm). (B) Cross-sections through the mechanosensitive dendritic tips of campaniform mechanoreceptors from the *Drosophila* haltere, depicting the extracellular sheath, the cell membrane, microtubules, and membrane-microtubule connectors (MMCs, arrows). MMCs are present in NOMPC^{+} wild-type flies (left) but lost in *nompC*^{1} null mutants (NOMPC^{-}, middle). Expressing 29+29ARs-NOMPC in the null mutants via NOMPC-GAL4 restores the MMCs (NOMPC$^{29+29ARs}$, right) (scale bar: 20 nm). Lower panel: Close-ups of the MMCs (top) and respective MMC tracings (bottom). For each strain, examples with a small (left) and a large (right) microtubule-membrane distance are displayed (scale bar: 20 nm. Red lines highlight the MMCs structure). (C) Relative abundance of MMCs in NOMPC^{+}, NOMPC^{-}, and NOMPC$^{29+29ARs}$ flies, calculated as the fraction of microtubules that associate with MMCs. MMC abundances in NOMPC$^{29+29ARs}$ flies resemble those in NOMPC^{+} flies ($p > 0.05$), and both differ significantly from the abundance in NOMPC^{-} flies that lack NOMPC protein ($p < 0.001$, two-tailed Mann-Whitney U-tests with Bonferroni correction; numbers of analyzed campaniform receptors: 31 (NOMPC^{+}), 24 (NOMPC^{-}), and 41 (NOMPC$^{29+29ARs}$)). (D) Upper left: Length distribution of the MMCs in NOMPC^{+} (n = 267) and NOMPC$^{29+29ARs}$ rescue flies, in which wild-type NOMPC is replaced with NOMPC$^{29+29ARs}$ (n = 307). Upper right: Respective distribution of the membrane-microtubule distance (n = 261 and 306, respectively). Lower left: membrane-microtubule distance in NOMPC^{+} (n = 261) compared with that of NOMPC^{-} flies (n = 310). Lower right: membrane-microtubule distance in NOMPC^{-} mutants compared with that of NOMPC$^{29+29ARs}$ flies. Filaments and distances were measured as depicted by the insets. ***: significant differences ($p < 0.001$; two-tailed Mann-Whitney U-tests with Bonferroni correction). Numbers of analyzed campaniform receptors as in panel C. All error bars denote ± s.e.m.. See also Figure S4.

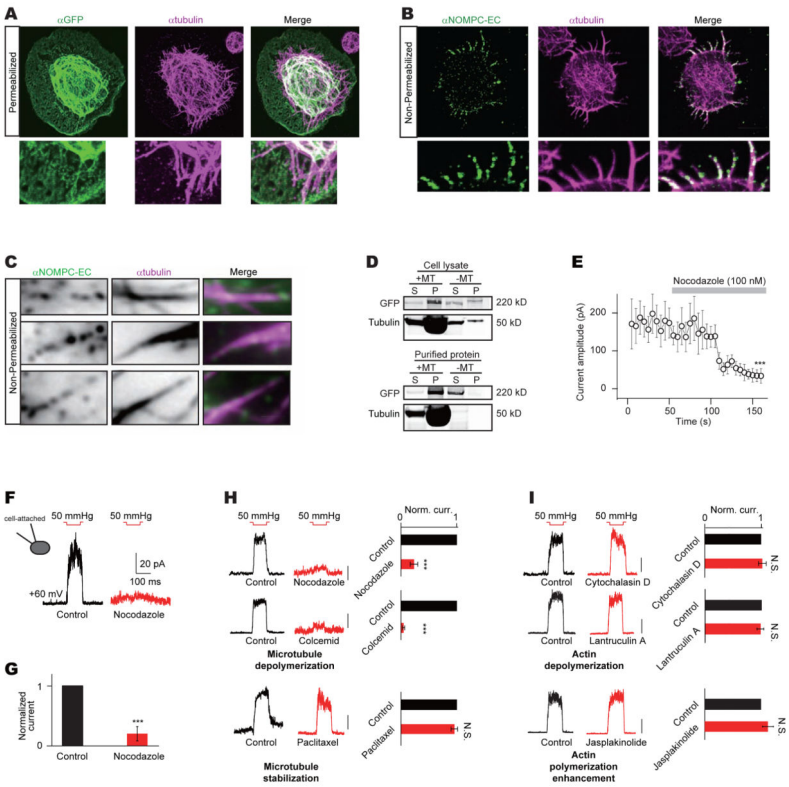

Figure 5. NOMPC channel's association with microtubules is important for mechanogating

(A) Staining of NOMPC and microtubules in NOMPC transfected S2 cells (scale bar: 5 μm). A focal plane of 0.35 μm was taken near the coverslip surface. (B) Staining of surface expressed NOMPC and microtubules in NOMPC transfected S2 cells (scale bar: 5 μm). A focal plane of 0.35 μm was taken near the coverslip surface. (C) TIRF microscopy showed interaction between membrane NOMPC and microtubules near the cell cortical area (scale bar: 1 μm). (D) Co-sedimentation assay of NOMPC form cell lysate or affinity purification with tubulin (+MT: with tubulin; -MT: without tubulin. S: Supernatant; P: Pellet). (E) Time course of nocodazole blockage of NOMPC's mechanogated current (paired *t*-test between time 0 s and 150 s, ***P3<30.001, n = 6). (F and G) Nocodazole (100 nM) blockage of NOMPC's mechanogated current at cell-attached mode (***P3< 0.001, paired *t*-test, n = 6 and 6). Membrane patches were held at +60 mV. (H) An inside-out patch with NOMPC channels show mechanogated current (Norm. curr.: Normalized current) to negative pressure of 50 mmHg at +60 mV. This current was reduced by adding nocodazole (100 nM, n = 7) or cochemid (10 μM, n = 6) but not paclitaxel (10 nM, n = 6) to the saline (scale bar: 50 pA. ***P <30.001, N.S.: not significant, paired *t*-test). (I) The mechanogated current of NOMPC to negative pressure of 50 mmHg at +60 mV was not effected by adding cytochalasin D (10 nM, n = 6), latrunculin A (1 μM, n = 6) or jasplakinolide (100 nM, n = 7) to the saline (scale bar: 50 pA. N.S.: not significant, paired *t*-test). See also Figure S5.

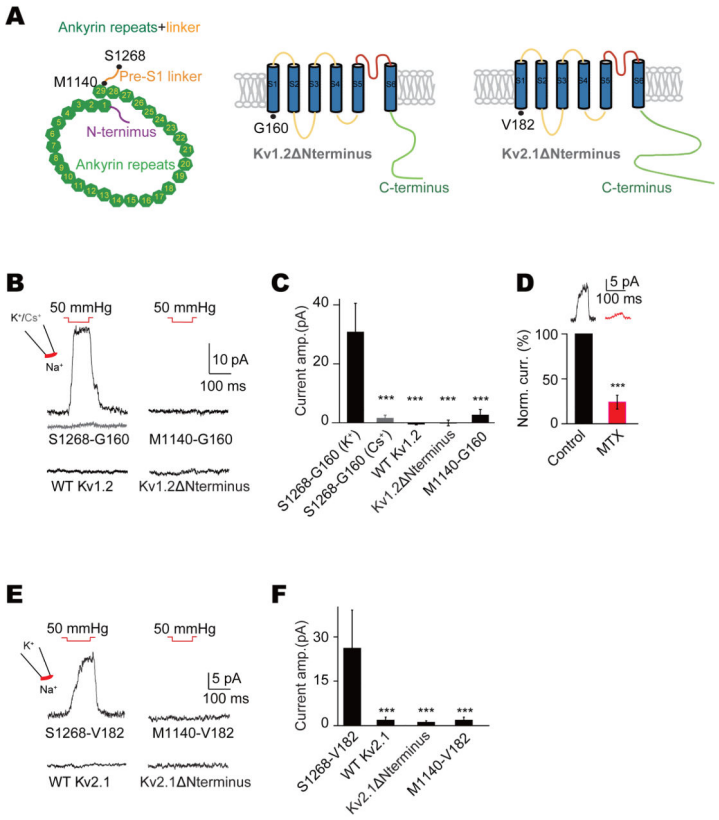

Figure 6. Ankyrin repeats from NOMPC confer Kv channels mechanosensitivity

(A) Strategy of constructing chimeric channels between NOMPC and Kv1.2 or Kv2.1. Amino acids defining the borders of protein fragments are highlighted with black dots. (B) Chimeric channel S1268-G160-Kv1.2 exhibited mechanogated current to membrane deformation caused by negative pressure, which was absent in Cs^+ solution (grey trace), while full-length Kv1.2 (WT Kv1.2), Kv1.2 with truncated N-terminus (Kv1.2ΔNterminus) and M1120-G160-Kv1.2 chimeric were not responsive to the same stimulus. Outside-out membrane patches were held at 60 mV. (C) Plots of mechanogated current amplitudes (n = 26, 8, 10, 7 and 7. One-way analysis of variance followed by Tukey's comparison for analyses of multiple groups. ***P < 0.001). (D) Mechanogated current was partially blocked with maurotoxin (MTX) (***P < 0.001, paired *t*-test, n = 6). (E) Chimeric channel S1268-V182-Kv2.1 exhibited mechanogated current to membrane deformation caused by negative pressure, while full-length Kv2.1 (WT Kv2.1), Kv2.1 with truncated N-terminus (Kv2.1ΔNterminus) and M1120-V182-Kv2.1 chimeric were not responsive to the same stimulus. Outside-out membrane patches were held at 60 mV. (F) Plots of mechanogated current amplitudes (n = 20, 7, 7 and 7. One-way analysis of variance followed by Tukey's comparison for analyses of multiple groups. ***P < 0.001). All error bars denote ± s.e.m.. See also Figure S6.

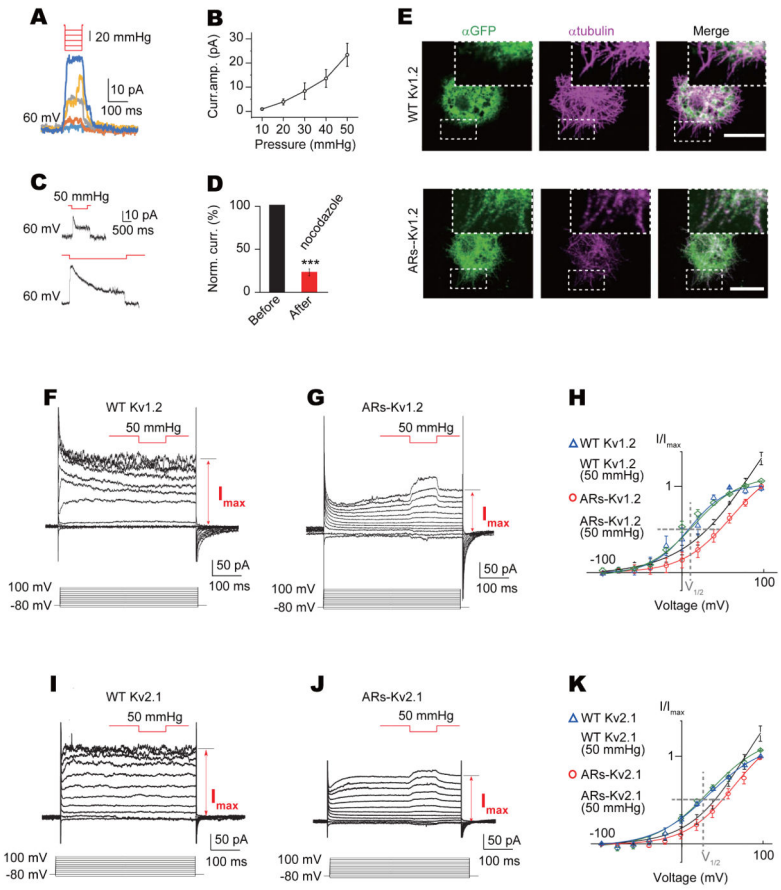

Figure 7. Biophysical properties of mechanosensitive chimeric channels

(A) Mechanogated current amplitude of ARs-Kv1.2 (S1268-G160-Kv1.2) chimeric channel increased with higher pressure (pressure ranged from 10 mmHg to 50 mmHg with 10 mmHg increment). (B) Dose-dependent curve of mechanogated current of ARs-Kv1.2 to pressure (n = 6). (C) Mechanogated current from ARs-Kv1.2 chimeric channel showed adaptation to prolonged stimulation. Membrane patches were held at 60 mV. (D) Mechanogated current from ARs-Kv1.2 chimeric channel was blocked by nocodazole (n = 6, ***P < 0.001). (E) Co-labelling of WT Kv1.2 channel and ARs-Kv1.2 chimeric channel with microtubules (scale bar: 5 μm, boxes highlighting microtubule filaments). (F and G) Representative current traces of WT Kv1.2 (F) and ARs-Kv1.2 chimeric channel chimeric channels (G) with pressure application during depolarization. (H) I–V curves of WT Kv1.2 and ARs-Kv1.2 chimeric channel with or without mechanical stimulation, normalized to current without mechanical stimuli at +100 mV (grey dash lines highlighting the I–V relationship at $V_{1/2}$). Membrane patches were held at −80 mV (n = 4 for each condition). (I and J) Representative current traces of WT Kv2.1 (I) and ARs-Kv2.1 (S1268-V182-Kv2.1) chimeric channel (J) with pressure application during depolarization. (K) I–V curves of WT Kv2.1 and ARs-Kv2.1 chimeric channel with or without mechanical stimulation, normalized to current without mechanical stimuli at +100 mV (grey dash lines highlighting the I–V

relationship at $V_{1/2}$). Membrane patches were held at −80 mV (n = 4 for WT Kv2.1 and 5 for chimeric channel). All error bars denote ± s.e.m.. See also Figure S7.